metals

MDPI

Article

Electrical Properties of Iodine-Doped Cu/f-CNT Coated Aluminum Wires by Electrophoresis with Copper Sulfate Solution

Fabrício Rodrigues [1,2,*], Paula Pinheiro [1], Mário Sousa [1], Rômulo Angélica [3], Simone Paz [3] and Marcos Reis [1,2,*]

[1] Programa de Pós-Graduação em Engenharia de Recursos Naturais da Amazônia, Instituto de Tecnologia, Universidade Federal do Pará, Belem 66075-110, PA, Brazil; paulafabiolapp@gmail.com (P.P.); mariofisicaedson@gmail.com (M.S.)
[2] Faculdade de Ciências Exatas e Tecnologia, Universidade Federal do Pará, Abaetetuba 68440-000, PA, Brazil
[3] Programa de Pós-Graduação em Geologia e Geoquímica, Instituto de Geociências, Universidade Federal do Pará, Belem 66075-110, PA, Brazil; angelica@ufpa.br (R.A.); paz@ufpa.br (S.P.)
* Correspondence: fab@ufpa.br (F.R.); marcosallan@ufpa.br (M.R.)

Abstract: This work investigated the effects of iodine on copper/functionalized carbon nanotubes (Cu/f-CNT) that were used in the coating of 1350 Aluminum Alloy wires, using the process of electrophoretic exposure with a solution of copper sulfate and iodine, under an electrical current of 1.2 A and a voltage of 10 V. The Al@Cu/f-CNT was characterized by Scanning Electron Microscopy in Secondary Electron mode, X-ray Diffraction and Raman spectroscopy, in addition to electrical measurements, at room temperature and under heating, via kelvin bridge. The results showed an increase of approximately 18% in the electrical conductivity of the IACS compared to the standard aluminum conductor, due to the iodine doping of the outer walls of the f-CNT, causing an expansion between the layers, and reflecting the increase in the conduction channels. This method of electrodeposition of Cu/f-CNT on the surface of metallic wires shows promise for the production of nanostructured cables with high ampacity, lightness and high performance, for application in power transmission lines.

Keywords: electrophoresis coating; nanostructured conductor cables; multiwalled carbon nanotubes; functionalization; iodine-doping

check for updates

Citation: Rodrigues, F.; Pinheiro, P.; Sousa, M.; Angélica, R.; Paz, S.; Reis, M. Electrical Properties of Iodine-Doped Cu/f-CNT Coated Aluminum Wires by Electrophoresis with Copper Sulfate Solution. *Metals* **2022**, *12*, 787. https://doi.org/10.3390/met12050787

Academic Editor: Michael R. Koblischka

Received: 25 February 2022
Accepted: 1 April 2022
Published: 3 May 2022

Publisher's Note: MDPI stays neutral with regard to jurisdictional claims in published maps and institutional affiliations.

Copyright: © 2022 by the authors. Licensee MDPI, Basel, Switzerland. This article is an open access article distributed under the terms and conditions of the Creative Commons Attribution (CC BY) license (https://creativecommons.org/licenses/by/4.0/).

1. Introduction

The development of new materials based on copper/functionalized carbon nanotubes (Cu/f-CNT) has attracted the attention of researchers due to their excellent mechanical strength properties, and high electrical and thermal conductivity [1–3], with expectations of applications in interconnections [1,4], portable electronics [5], silicon chip development [3] and the development of new nanostructured electrical conductors [2,6]. CNT exhibit excellent electron emission properties, electrical conductivity from 10^7 to 10^9 A/cm^2, low density, and good mechanical performance with their Young's modulus and tensile strength being in the range of 1.0 TPa and 50 GPa, respectively [7,8], and thermal conductivities from 2000 to 7500 W/mK [8–13] have been demonstrated for multiwalled carbon nanotubes (MWCNT). Copper, with its high electrical conductivity, high current-carrying capacity, strength and corrosion resistance is considered an ideal detection material due to its good stability and electrocatalytic properties, but its high density is a disadvantage [14,15]. Aluminum and its alloys are lighter but have a lower melting point and are more inclined to oxidation than copper, in addition to having a lower current-carrying capacity [16].

Cu/CNT systems are promising candidates for the manufacture of more efficient conductor cables, with high ampacity, low density, a coefficient of thermal expansion comparable to that of silicon [17], in addition to high mechanical strength and corrosion resistance [6,18]. Fabrication of such material can be achieved by a variety of methods, including Electrophoretic Deposition (EPD) routes [19–21], electroplating [22,23], powder

metallurgy [24], conventional casting [9], solubilization and heat treatment. Rodrigues, et al. studied nanostructured coating processes on aluminum substrates of alloy 6101 with CNT using a solubilization process followed by heat treatment at a temperature of 550 °C and aging at 180 °C, resulting in a reduction in electrical resistance of 13.7% compared to the conventional cables [25]. However, challenges are faced for a good deposition; for example, the strong tendency of CNT to agglomerate, making uniform dispersion in the matrix difficult, in addition to the low interaction between the matrix and the CNT [9], are recurring problems for most processing techniques. For electrophoretic deposition, which is a well-known colloidal processing method that is gaining increasing interest as a simple and versatile technique for the manipulation and deposition of nanoparticles and CNT [17,21,26], some parameters must be analyzed, such as: deposition time, electric field, electrode materials, CNT functionalization [17,27,28], doping [6,29], and suitable suspensions for EPD [9,28]. Recently, Rodríguez-Salinas, et al. [29] used the EPD process to perform electroplating of functionalized MWCNT on the surface of aluminum alloy 6061 (AA 6061), achieving an increase of 9.6% in the electrical conductivity of the nanostructured wire compared to the conventional wire.

New Cu/CNT coated aluminum conductors are part of a new generation of advanced materials with high performance, which represents a great alternative to solve serious problems faced by the electric sector, where great technical losses are generated in the transmission and distribution of electric energy [30]; for example, hot spots, corrosion in connections and cables (as conventional metallic conductors suffer significant degradation or complete failure in their performance when subjected to severe oxidation environments) [18,30], mechanical failures, electromigration [31,32], hysteresis (caused by Foucault currents) and losses (caused by the Joule effect) [33] are problems that lead researchers to research more efficient and viable approaches to power generation and transmission [7]. In developing countries, it is estimated that about 20% of power losses occur in transmission and distribution networks [34]. In Brazil, in 2020, technical losses reached 7.5% and generated a cost of around US$ 1.6 billion (obtained by multiplying the values by the average price of power in the tariff processes, without considering taxes) [35]. In this scenario, conductors based on nanocomposites offer advantageous properties compared to conventional conductors based on metals and their alloys; these advantages include lower weight, greater load capacity and better resistance to mechanically or chemically aggressive environments [36].

2. Experimental Procedure

2.1. Materials

Commercial 1350 aluminum alloy (AA 1350) wires (with dimensions of 250 mm in length and 2.7 mm in diameter), manufactured by ACL Cables PLC (Colombo, Sri Lanka), were used as substrates for the nanostructure coating. Functionalized MWCNTs with carboxylic acid (-COOH), with ≥95% purity, were provided by the Federal University of Minas Gerais. Electrophoretic solutions were prepared using: resublimated iodine PA (DINÂMICA, Indaiatuba, Brazil), copper sulfate (ICO) $5H_2O$ PA-ACS (98% purity), Dimethylformamide surfactant (DMF, 99.8%), acetone PA, sodium hydroxide (all purchased from SYNTH, Diadema, Brazil) and distilled water. The electrical voltage was applied by a DC voltage source (regulated power supply-MPL3303M, 0–30 V, 5A from the manufacturer MINIPA, Joinville, Brazil). A model 752A magnetic stirrer (FISATOM, Sao Paulo, Brazil) with a capacity of 4 L, a rotation range from 100 to 1800 rpm and optional heating up to 360 °C was used to stir the electrolyte solution. A model L100 ultrasonic washer (SCHUSTER, Santa Maria, Brazil), with a frequency of 50/60 Hz was used to disperse the electrophoretic solution. A microprocessed drying oven, model SX1.0DTMS (STERILIFER, Sao Caetano do Sul, Brazil), made of 430 stainless steel was used to dry the wires.

2.2. Wire Coating Process

Figure 1 schematically illustrates the process of coating the AA 1350 wire with copper/functionalized carbon nanotubes (Al@Cu/f-CNT). Initially, wire (as received) was submerged (I) for 20 s in an aqueous solution of sodium hydroxide (NaOH) and washed with distilled water to remove surface impurities before coating with copper via electrolysis. This deposition (II) was carried out using a conventional bath of copper sulfate ($CuSO_4$) with a concentration of 2 mg/mL under magnetic stirring, containing aluminum wire (acting as an anode) and a copper bar (acting as a cathode), under an electrical voltage of 0.5 V for 5 min, followed by drying in an oven at 50 °C for 20 min, and the Al@Cu wire was thus produced.

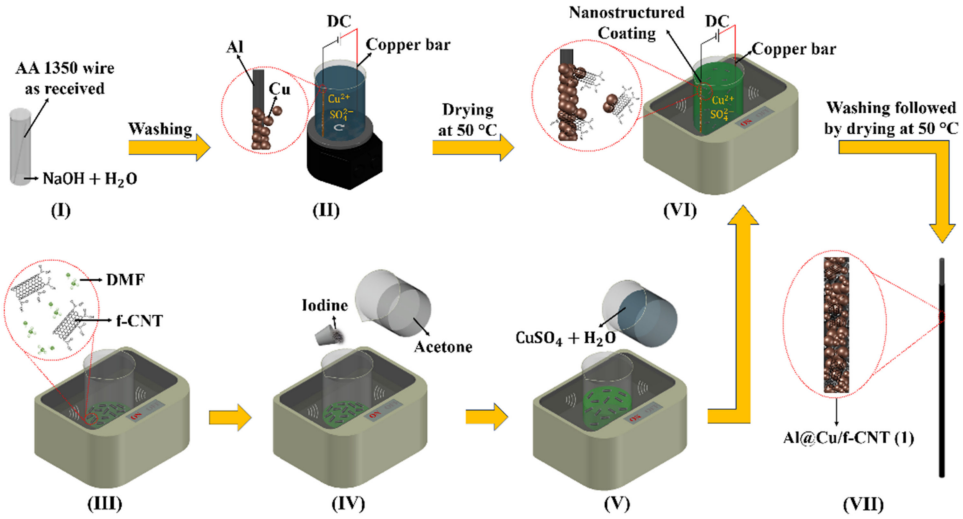

Figure 1. Schematic illustration of AA 1350 wire-coating process with Cu/f-CNT.

The f-CNT were dispersed (III) in DMF at the proportion 20:1 with the aid of an ultrasound bath at 40 Hz for 24 h, followed by the addition (IV) of 200 mL of acetone and 10 mg of iodine. Additionally, a solution of copper sulfate and distilled water in the proportion of 1:2 with a volume of 300 mL was deposited (V). This mixture of solutions was subjected to an ultrasonic bath for 60 min and then used as an electrophoretic bath. The nanostructured coating was added by electrophoresis (VI), with the Al@Cu wire (anode) and the copper bar (cathode) inside the electrophoretic solution for 8 min at 1.2 A and 10 V, followed by washing in distilled water and drying at 50 °C for 30 min, thereby producing the (VII) Al@Cu/f-CNT (1) wire.

2.3. Sample Characterization

The morphological characterization of the Al@Cu/f-CNT (1) wire was performed by Scanning Electron Microscopy (SEM) using a microscope model VEGA3 (TESCAN, Brno, Czech Republic) in secondary electron mode, with acceleration voltages of 10 and 30 kV and working distances of 9.71 and 9.72 mm. The crystallinities and crystallographic orientation, in addition to the FWHM, of the f-CNT, Al@Cu and Al@Cu/f-CNT (1) samples were characterized by X-ray Diffraction (XRD) using an EMPYREAN Co model diffractometer (Kα1 = 1.789010 Å) and a PIXCEL3D-Medpix3 1 × 1 detector (both manufactured by MALVERN PANALYTICAL LTD., Malvern, England) with anodic X-ray tubes, fine focus and Fe Kβ filter, in a 40 kV voltage mode and with a current of 35 mA. The X-ray wavelength was 0.1790 nm and the samples were analyzed in powder form after scraping the coatings from the wires.

The vibrational characterization of the f-CNT and Al@Cu/f-CNT (1) powder samples was performed using a Raman spectrometer model T64000 (HORIBA JOBIN YVON, Bensheim, Germany) with a charge-coupled device (CCD) for signal detection, by means of scattered retro-geometry. The samples were analyzed in an environment with a 532 nm

(2.33 eV) laser line focused on the sample surface using a SLMPlan N 20 × /0.25 objective lens (OLYMPUS, Tokyo, Japan). For comparison, a sample of an Al wire was coated with Cu/f-CNT via electrophoresis at 1.5 A and 16 V for 8 min, and this was labelled as Al@Cu/f-CNT (2).

The electrical characterization of the AA 1350, Al@Cu/f-CNT (1) and Al@Cu/f-CNT (2) wires, at room temperature, was performed using a digital multi-ohmmeter MPK-2000e (MEGABRAS, Sao Paulo, Brazil) to measure the resistances and calculate the electrical resistivity and electrical conductivity of the IACS following the ASTM B3-13(2018) [37] and ASTM B193-20 [38] standards. Electrical characterization, under temperature variation, was performed by heating the wires using a heat source with a power of 250 W, while the electrical resistances were monitored with an MD-6111 digital multimeter (ICEL, Manaus, Brazil) using a Kelvin bridge powered by a DC MPL-3303M source (MINIPA, Joinville, Brazil). The tested wires had a length of 250 mm and the temperature variation in the wires was monitored with a TD-955 infrared thermometer (ICEL, Manaus, Brazil).

3. Results and Discussions

3.1. Coated Wire Morphology

Figure 2 shows the SEM micrograph of the Al@Cu/f-CNT (1) wire, which was coated, via electrophoretic deposition, with an electric current of 1.2 A for 8 min. Figure 2a shows SEM micrographs with magnification of 2000×, indicating that the deposition of Cu/f-CNT on the aluminum substrate occurred in a predominantly homogeneous way, forming a coating with a thickness of approximately 13 μm, which was close to that obtained by Reis, et al. [39] using a similar process of electrodeposition.

The surface uniformity of the Al@Cu/f-CNT (1) wire is a consequence of the combination of the DMF treatment, which presents better suspension stability and has good performance during the electrophoretic deposition (EPD) of MWCNT [40], with the improvement of the interaction between the aluminum surface and the Cu/CNT coating due to the functionalization of CNT [17,41,42] and its doping with iodine. The iodine added to the solution acts as a positive load and increases the surface load of the f-CNT [43], in addition to acting as a doping element that can lead to fundamental improvements in the conductance of the iodine-doped CNT system [6].

The SEM micrograph of Figure 2b, corresponding to the region highlighted in the yellow rectangle of Figure 2a, shows at 10,000× magnification the formation of morphological pyramidal structures with square bases (yellow arrow), demonstrating that the electrophoretic deposition occurred at a low rate of copper nucleation on the wire surface, without the occurrence of hydrogen evolution. Li, et al. [44] stated that the evolution of hydrogen in the electrodeposition forms tiny flows of hydrogen as a dynamic model and, therefore, influences the morphology of the deposited copper layers. Thus, hydrogen bubbles can cause the coating to peel, in addition to favoring the formation of structures in the form of nanosheets [45,46] as well as dendritic copper structures consisting of a main stem with long lateral branches [46]. Furthermore, Figure 2c, showing an image taken at 10,000× magnification over the region highlighted in the light blue rectangle in Figure 2b, reveals CNT (white arrow) completely coated with copper with initial points of agglomeration. On the other hand, in Figure 2d, showing an image taken with a magnification of 50,000× over the area delimited by the red rectangle in Figure 2b, CNT (white arrow) can be observed on the prismatic face of a Cu crystal (white arrow).

3.2. Crystal Structures

Figure 3 shows the XRD results of the f-CNT (dark green line), Al@Cu (blue line) and Al@Cu/f-CNT (1) (red line) samples between 20° and 65° (2θ). In the f-CNT sample, position A, located at 2θ around 26°, corresponds to the typical diffraction peak of the graphitic hexagonal structure with a (002) orientation. Position B, near 43°, corresponds to graphitic planes with a (100) orientation [47].

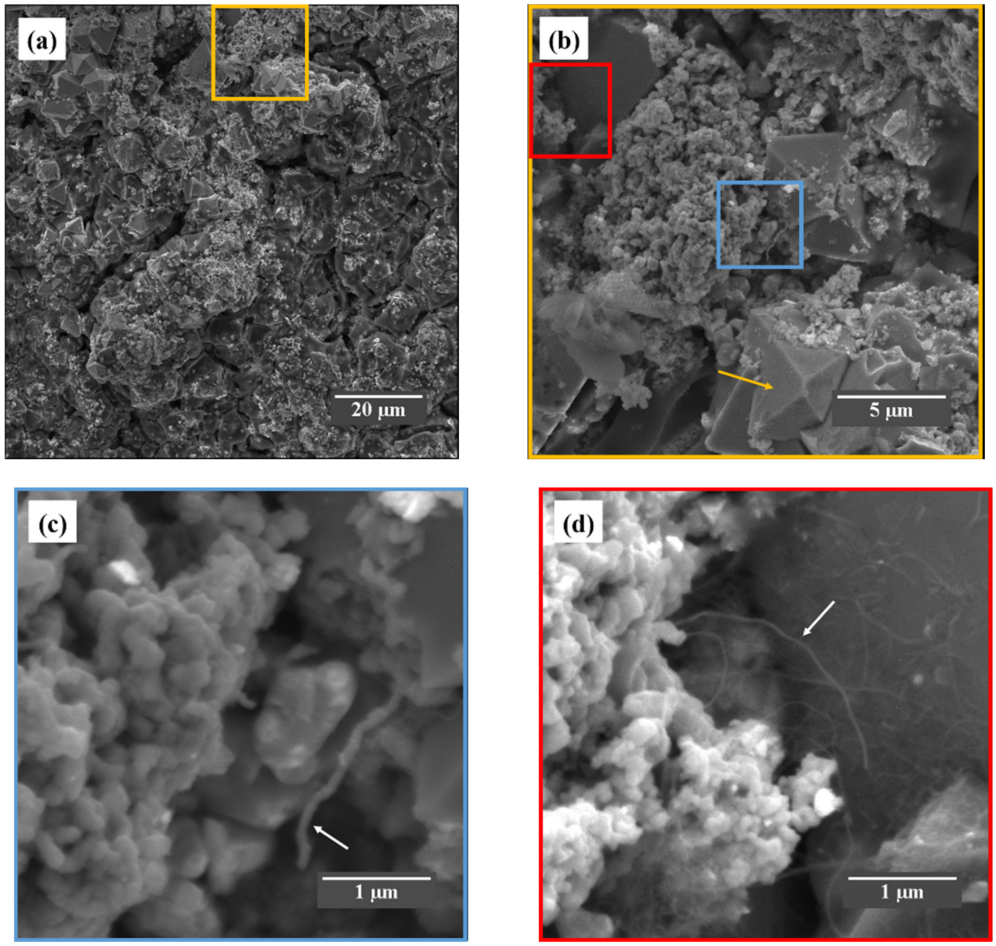

Figure 2. Al@Cu/f-CNT (1) wire morphology: (**a**) SEM micrograph at 2000× magnification showing a predominantly homogeneously deposited coating. (**b**) 10,000× magnification in the region of (**a**) highlighted in the yellow rectangle revealing pyramidal copper structures (yellow arrow). (**c**) 50,000× magnification in the region of (**b**) highlighted in light blue rectangle. (**d**) 50,000× magnification in the region of (**b**) highlighted in red rectangle. In (**c**) clustered copper crystals are observed coating f-CNT (white arrow), while in (**d**) f-CNT (white arrow) are found only on one of the prismatic faces of Cu.

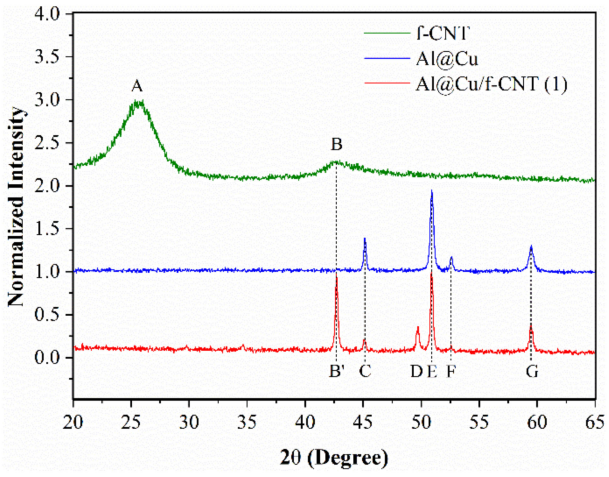

Figure 3. XRD patterns of f-CNT, Al@Cu and Al@Cu/f-CNT (1) samples.

Two diffraction peaks for the Al@Cu sample can be clearly recognized in the spectrum grown mainly in the crystallographic orientations (200) and (220) corresponding to the copper diffraction plane at 2θ = 50.92° (E position) and 2θ = 59.54° (position G), respectively. Diffraction peaks corresponding to aluminum were observed mainly in the crystallographic orientation (200) at 2θ = 45.20° (position C), and also appeared at position F (52.60°) [48,49]. Note that the grain growth was superior in the direction (111) of copper, indicating that the voltage parameters and electrodeposition time (0.5 V and 5 min, respectively) were not enough to favor grain growth in this direction during the conventional coating. According to research by Mladenović, et al. [50], the increase in current density in the electrodeposition of copper films results in the preferential change from strong (220) to strong (111). On the other hand, in some cases of low voltage electrodeposits, the orientation (111) does not appear.

All copper and aluminum peaks in the Al@Cu sample were observed in the Al@Cu/f-CNT (1) sample. However, there was a reduction in the intensity of aluminum peaks (indicating lower substrate diffraction). We observed the appearance of peaks D and B′, where the peak D corresponds to a Miller index (311) of CuI in 2θ close to 50° [51] and indicates the interaction of copper with iodine (used in the doping of f-CNT) during the nanostructured coating process. Peak B′ (at 2θ = 42.68°) corresponds to Cu that grew in the (111) direction, due to longer time and greater current density, which could possibly be attributed to the preferential adsorption of CNT on Cu (111). This intense adsorption prevents further reductions in copper ions on Cu faces (111) and promotes lateral film growth, resulting in 2D copper thin films with smooth surfaces [46], which can result in the suppression of the diffraction peak of the graphitic planes of the CNT. The SEM micrographs of Figure 2c show that the copper structures were enveloped the CNT, and this also caused the suppression of peak A. Similar behavior was reported for MWCNT-COOH surrounded by Fe_3O_4 [47].

X-ray diffraction patterns were used to determine the crystallite size (d), which was estimated by means of line-broadening measurements obtained using the Debye–Scherrer equation, given in Equation (1). In this equation, λ is the wavelength of the X-ray in nanometers (nm) (equal to 0.1790 nm), β is the half-height width of the diffraction peak (FWHM), and K is a constant related to the crystal form (equal to 0.9 at most) [52].

$$d = K\,\lambda/\beta\,\cos\theta \quad (1)$$

The calculations of FWHM and crystallite size—presented, respectively, in Tables 1 and 2—showed that the crystallinity of the C and F peaks did not change significantly with the reduction in aluminum from 39.30 to 11.80% in the samples of Al@Cu and Al@Cu/f-CNT (1), respectively. Although the intensities of the E and G peaks of the Al@Cu/f-CNT (1) sample did not change in comparison to the Al@Cu sample, there was an increase in crystallinity and grain size, with a reduction in FWHM, possibly due to copper growth in orientation (111). Song, et al. [53] suggested that during the electrodeposition process, in any condition, copper ions are continuously reduced, and thus, Cu_2O is formed and then perfectly reduced to the metallic Cu phase, which improves the electrical and thermal conduction of the nanocomposites. Furthermore, Subramaniam, et al. [32] stated that CNT suppress primary copper failure pathways, increasing the activation of copper diffusion energy in Cu/CNT systems, which increases the crystallinity of the sample with CNT.

Table 1. FWHM values and percentage of Al in f-CNT, Al@Cu and Al@Cu/f-CNT (1) samples.

Samples	A	B	B′	C	D	E	F	G	Al (%)
f-CNT	4.5	4.1	-	-	-	-	-	-	0.0
Al@Cu	-	-	-	0.2336	-	0.3427	0.2549	0.4724	39.30
Al@Cu/f-CNT (1)	-	-	0.2532	0.2725	0.2997	0.2614	0.2817	0.3367	11.80

Table 2. Crystallite sizes and percentage of Al in f-CNT, Al@Cu and Al@Cu/f-CNT (1) samples.

Samples	A	B	B′	C	D	E	F	G	Al (%)
f-CNT	2.57	2.72	-	-	-	-	-	-	0.0
Al@Cu	-	-	-	34.40	-	23.45	31.52	17.01	39.30
Al@Cu/f-CNT (1)	-	-	34.07	35.79	29.54	34.04	31.80	27.47	11.80

3.3. Raman Scattering

The Raman spectra of f-CNT (as received) and nanostructured wires (named Al@Cu/f-CNT (1) and Al@Cu/f-CNT (2) when derived from electrophoresis at 1.2 A and 1.5 A, respectively) showed the presence of D and G bands in the range of 1200 cm^{-1} to 1700 cm^{-1}, while a 2D band was observed in the range of 2500 cm^{-1} to 3000 cm^{-1}, as seen in Figure S1 of the Supplementary Materials. These bands and their sub-bands are fundamental for understanding the influence of iodine-doped f-CNT in terms of improving the properties of metallic conductors. The Lorentzian deconvolutions showed the satellite peaks around the D band (D_L and D_R, where the subscripts L and R refer to the peaks to the left and right side of the D band, respectively, and D_{LO} denotes the longitudinal optical phonon component) and the D_{middle} peak, which were related to the degree of amorphous carbon in the sample [54–56]. The G band presented two major sub-bands, G_{inner} and G_{outer}, which occurred due to the stress/pressure of the CNT cluster, the radial stress/deformation in the carbon nanotube and the proximity of the CNT's innermost and outermost diameter distributions, respectively. The 2D band presented two sub-bands, known as $2D_{inner}$ and $2D_{outer}$, which were also related to the innermost and outermost diameter distributions of the MWCNT, respectively [54,55,57]. In addition, an association between the D_L + G and D_R + G components, with peaks from 2820 cm^{-1} to 3000 cm^{-1}, could provide new information about Raman scattering due to the electron deposition process [54,56] and revealed some information on the D band [58–60]. The positions of all peaks referring to the D and G bands (first-order Raman scattering) in addition to those referring to the 2D band (second-order Raman scattering) are described in Tables 3 and 4, respectively.

Table 3. The Raman peaks obtained from Lorentzian deconvolutions of the D and G bands.

Samples	D_{LA}	D_L	D_R	D_{LO}	D_{middle}	G_{inner}	G_{outer}	D′
f-CNT	1227	1340	1349	1369	1489	1578	1593	1619
Al@Cu/f-CNT (1)	-	1302	1346	1372	1478	1556	1585	1626
Al@Cu/f-CNT (2)	-	1314	1343	1364	1460	1567	1583	1611

Wave number of Raman peaks in cm^{-1}.

Table 4. The Raman peaks obtained from Lorentzian deconvolutions of the 2D band.

Samples	$2D_{inner}$	$2D_{outer}$	D_L + G	D_R + G	D″
f-CNT	2690	2701	2900	2949	2467
Al@Cu/f-CNT (1)	2691	2734	2881	2916	-
Al@Cu/f-CNT (2)	2679	2707	2923	2952	-

Wave number of Raman peaks in cm^{-1}.

The f-CNT sample presented a D_{middle} sub-band with a lower degree of amorphous carbon than the coated wire samples (as can be seen in the spectrum of Figure S1 in the Supplementary Materials). Figure 4 shows an evaluation of the effects on the outermost layers of MWCNTs determined through the ID_R/IG_{outer} ratio, where we observed that there was an increase from 1.47 (f-CNT) to 1.6 and 2.7 when comparing, respectively, with Al@Cu/f-CNT (2) and Al@Cu/f-CNT (1), indicating that after the electrodeposition process, there was an increase in the density of defects/disorders, mainly in the outer tubes of the MWCNT, and mainly for the Al@Cu/f-CNT (1) sample. As a result, there was an increase in the degree of amorphous carbon, as shown by the relative area of D_{middle} (amorphous carbon area, dark yellow) of Figure 4.

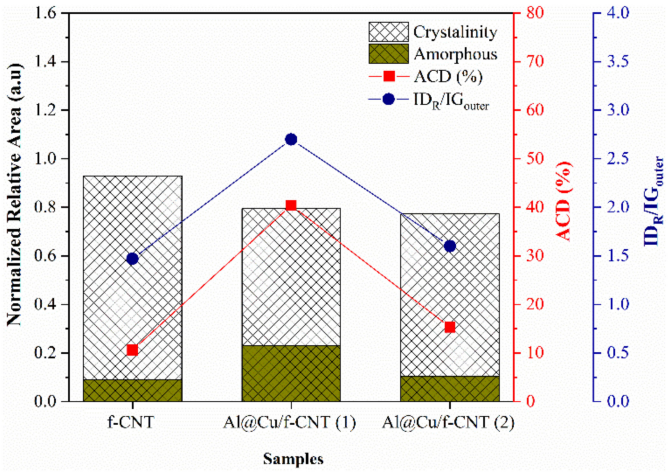

Figure 4. Peak intensity ratios related to defects and graphitization of the outermost tubes (dark blue balls) and the degree of amorphous carbon (red squares) obtained for different samples, with the relative areas normalized by the f-CNT area for crystallinity and amorphousness.

The relationship between the amount of amorphous carbon and the crystallinity of the carbon nanotubes, known as the Amorphous Carbon Degree (ACD) [55], was determined based on the rate of the integrated areas of the D_{middle} sub-band with respect to the G_{inner} and G_{outer} sub-bands, which referred to the sp^3 and sp^2 bond sites, respectively, according to Equation (2):

$$ACD = [\Sigma \text{ rel. area } (D_{middle})/\Sigma \text{ rel. area } (G_{inner} + G_{outer})] \times 100\% \quad (2)$$

where these sub-bands were shown from the Raman spectrum fit, as can be seen in Figure S1 of the Supplementary Materials.

Figure 4 also shows that the samples of Al@Cu/f-CNT (1) and Al@Cu/f-CNT (2) had, respectively, ACD values that were around 30 and 5% higher than that of the f-CNT sample, indicating that morphological changes occurred in the structure of the nanotubes with sp^2 to sp^3 binding losses during the preparation and electrodeposition steps. The Al@Cu/f-CNT (2) wire presented less amorphousness than the Al@Cu/f-CNT (1) wire, but the relative area of the crystallinity of the latter was 3.11% higher. In fact, as evidenced by the SEM micrographs of Figure S2 of the Supplementary Materials, a smoother surface was obtained in the electrodeposition coating at 1.2 A, while the current of 1.5 A did not favor the homogeneous dispersion of the coating on the substrate Al, forming a rough surface that, according to studies by Timoshevskii, et al. [61], reflected the increase in the electrical resistivity of the Al@Cu/f-CNT (2) wire compared to the Al@Cu/f-CNT (1) wire, as shown in Figure S3 of the Supplementary Materials.

Figure 5a shows the shifts of the G_{inner} and G_{outer} sub-bands, related to the tangential vibrations of the outermost and innermost layers of the MWCNT, respectively [57], of the samples Al@Cu/f-CNT (1) and Al@Cu/f-CNT (2) compared to the f-CNT sample. The G_{inner} and G_{outer} positions of the Al@Cu/f-CNT (1) wire, compared to the f-CNT sample, showed shifts for low frequencies (redshift) at around 22 cm^{-1} and 8 cm^{-1}, respectively, evidencing a process mediated by *n*-doping with a higher density of defects and, therefore, as illustrated in Figure 5b, with an average increase of 17 cm^{-1} e 28 cm^{-1} in the FWHM of the G_{inner} and G_{outer} sub-bands, respectively. The Al@Cu/f-CNT (2) sample also presented redshifts compared to the f-CNT sample, with these being at 11 cm^{-1} for G_{inner} and 10 cm^{-1} for G_{outer}. However, it must be noted that this was mediated by a lower defect density than the Al@Cu/f-CNT (1) sample, showing an average increase of 4 cm^{-1} and 3 cm^{-1} in the FWHM of the G_{inner} and G_{outer} sub-bands, respectively, evidencing that the doping effects were more intense for the Al@Cu/f-CNT (1) sample, reflecting improvements in the properties of the nanocomposite. In this process, the expansion of the layers of the

carbon tubes occurred, because of the effect of doping with iodine after the electrophoresis process. This effect was more expressive on the outermost layers of the tubes, mainly in the Al@Cu/f-CNT (1) wire, indicating that it suffered higher levels of doping with iodine. The expansion was generated by the repulsion between charged negatively layers caused by a polar interaction with iodine on the outermost walled sheets of the CNT, promoting a separation of the carbonaceous layers.

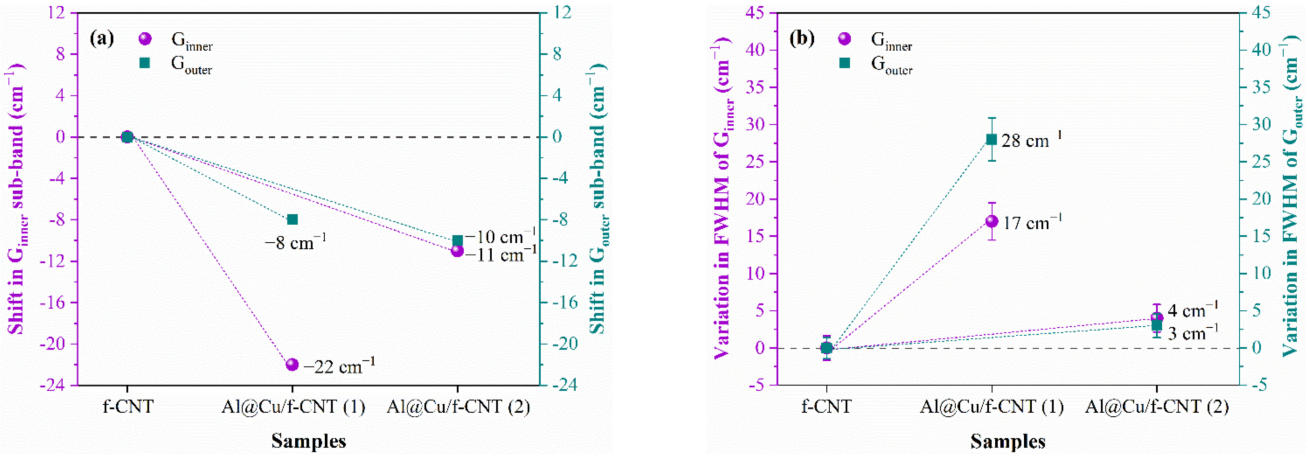

Figure 5. (**a**) Shifts and (**b**) FWHM variations of the G_{inner} and G_{outer} sub-bands of the Al@Cu/f-CNT (1) and Al@Cu/f-CNT (2) samples compared to the f-CNT sample as received.

The degree of charge transfer between the donor (copper) after oxidation and the f-CNT may be defined by the quantity *f*, which is the transferred charge per host C atom [62]. Using stages of 1.2 A and 1.5 A with respect to the f-CNT sample, and using an average transfer charge $\Delta\omega/\Delta f \approx 460 \pm 6$ cm^{-1} for the Al@Cu/f-CNT (1) sample, a value of $f \approx 1/57$ was obtained, indicating the transferred charge of one free hole per host 57 C atom of the G_{outer} component, which suggested that there was an increasing charge transfer into the π band that corroborated the redshift in the G_{outer}.

Figure S3a of the Supplementary Materials shows the shifts of the $2D_{inner}$ and $2D_{outer}$ sub-bands of the Al@Cu/f-CNT (1) and Al@Cu/f-CNT (2) samples compared to the f-CNT sample, revealing that the charge doping in the system was associated with the electrophoretic obtaining and deposition processes of the wires. In comparison to the as-received f-CNT sample, the Al@Cu/f-CNT (1) wire presented blueshifts of 1 cm^{-1} and 33 cm^{-1} for the $2D_{inner}$ and $2D_{outer}$, respectively, demonstrating strain mainly in the distribution of the outermost tubes. In contrast, the Al@Cu/f-CNT (2) wire had a redshift of 11 cm^{-1} for $2D_{inner}$ and a blueshift of 6 cm^{-1} for $2D_{outer}$. In fact, a loss or gain of charge resulted in the compression and expansion of the crystal lattice of the nanotubes that occurred during the Cu/f-CNT electrodeposition mechanism on the aluminum substrate, characterizing an *n*-doping and *p*-doping process, respectively. In this sense, Figure S3b of the Supplementary Materials shows that, compared to the f-CNT sample, the $2D_{inner}$ FWHM increased by an average of 7 cm^{-1}, while the $2D_{outer}$ FWHM decreased by an average of 9 cm^{-1} for the Al@Cu/f-CNT (1) wire, with these being related to the ionic potential of the diameter distributions [63]. In the Al@Cu/f-CNT (2) wire, the FWHM of $2D_{inner}$ and $2D_{outer}$ were reduced by an average of 26 cm^{-1} and 12 cm^{-1}, respectively, compared to the FWHM values of the f-CNT sample (60 cm^{-1} for $2D_{outer}$ and 84 cm^{-1} for $2D_{inner}$).

3.4. Electrical Behavior of Conventional and Nanostructured Wires

Commercial conductive wires used in power distribution and transmission lines are made of aluminum alloy 1350 (AA 1350), aluminum alloy 1120 (AA 1120) and aluminum alloy 6201A (AA 6201A), which have an IACS conductivity of 61%, 59% and 53%, respectively [64]. In this work, AA 1350 wires were used as substrates to be coated with

Cu/f-CNT. As shown in Figure 6a, this nanostructured coating resulted in superior electrical conductivities compared to conventional AA 1120, AA 6201A and AA 1350 alloys at room temperature. The Al@Cu/f-CNT (1) wire (coated by electrophoresis at 1.2 A) showed an IACS conductivity of 72.93 ± 0.63%, while the Al@Cu/f-CNT (2) wire (coated by electrophoresis at 1.5 A) showed an IACS conductivity of 64.54 ± 0.88%, which corresponded to increases in electrical conductivity of approximately 18% and 4.3%, respectively, compared to the AA 1350 wire. Rodríguez-Salinas, et al. [29] reported an IACS electrical conductivity of 47.7 ± 1.93% for AA 6061 coated with undoped f-CNT (AA 6061@f-CNT) by electrodeposition and, thus, managed to achieve an improvement of 9.6% in comparison to the uncoated alloy. This improvement, however, proved to be almost twice as low as that obtained for Al@Cu/f-CNT (1) wire, suggesting that the Cu/f-CNT system, as well as iodine doping, further increase the carrier concentration and mobility within CNT bundles [6,43,65]. The iodine that remained on the surface of CNT had a relatively strong chemical bond and promoted an increase in conduction in conjunction with the properties of CNT [6]. Li and Fahrenthold [28] demonstrated through computer modeling that the conductance of iodine-doped CNT is affected by the concentration and distribution of the dopant, promoting metallic conduction to the system due to the formation of polyiodide structures [6,28,66,67], in addition to the creation of doped conduction "pathways" (axial asymmetric doping) in nanotubes and conduction in polyiodide chains, through a Grothuss mechanism [28]. Furthermore, the local electrostatic Coulomb cohesion between the CNT beams, due to the dipole moments induced at the surface, promoted an increase in electrical and thermal conductance that was almost 2.8 times greater than the non-functionalized counterpart [68].

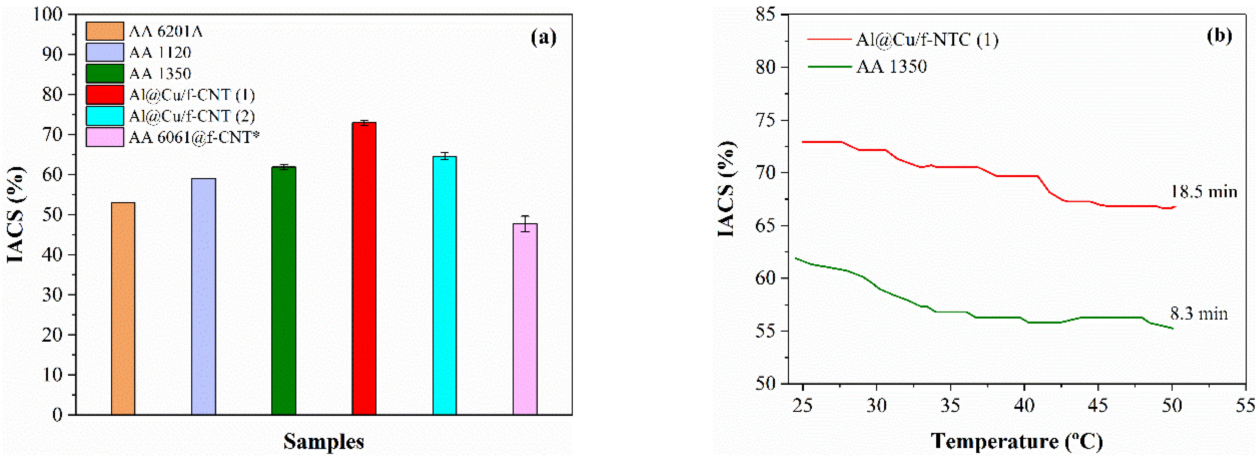

Figure 6. (**a**) Comparison between the IACS values of conventional AA 6201A, AA 1120 and AA 1350 wires with nanostructured Al@Cu/f-CNT (1), Al@Cu/f-CNT (2) and AA 6061@f-CNT wires, at room temperature. (**b**) Comparison between the IACS values of samples AA 1350 and Al@Cu/f-CNT (1) measured as a function of heating from 25 to 50 °C. AA 1120 and AA 6201A values extracted from [64]. *AA6061@f-CNT values extracted from [29].

Additionally, the resistivity results presented in Figure S4 of the Supplementary Materials prove that the Al@Cu/f-CNT (1) wire showed a decrease of 3.29×10^{-9} Ωm compared to the resistivity of the AA 1350 wire, while the Al@Cu/f-CNT (2) wire had a reduction of only 0.85×10^{-9} Ωm. According to Timoshevskii, et al. [61], rough structures, as seen in the Al@Cu/f-CNT (2) wire, tend to cause interleaf electron scattering on the Fermi surface, in which case one or more Bragg planes cut the Fermi surface in this direction and the Fermi surface is slit open at the points of intersection. The size of these cracks is determined by the strength of the roughness potential of the disturbing surface. This effect should reduce the projected Fermi surface area and, thus, drastically reduce the electrical conductivity of thin films. Thus, it is noted that while the better dispersion of nanotubes in the solution can increase the conduction channels and suppress possible failures resulting

from the electrodeposition [32], the increase in the electric current can be unfavorable to the electrophoretic coating process and, consequently, suggest low improvement in the electrical conductivity of Al@Cu/f-CNT (2) wire compared to standard AA 1350 wire.

Figure 6b compares the electric conductivity of the AA 1350 and Al@Cu/f-CNT (1) samples during heating from 25 °C to 50 °C. The IACS conductivity of the AA 1350 conductor was reduced from 61.89 to 55.26% in 8.3 min, while that of the nanostructured wire was reduced from 72.89 to 66.80% in 18.5 min. Thus, both wires demonstrated a predominance of the metallic conduction mechanism over the tunneling and hopping conduction mechanism. Note that although the thermal excitation caused the scattering of electrons in copper and aluminum, the carbon nanotubes (with their high thermal conductivity) and the thermal vibrations in the functional groups attached to their surface [68], as well as the iodine doping, continued to favor the formation of conduction channels, causing the conductivity of the Al@Cu/f-CNT (1) wire at 50 °C to remain 5.79% IACS higher than that obtained for the AA 1350 wire at room temperature. Moreover, the thermal conductivity of aluminum is mostly electronic, while the thermal conductivity of Cu/CNT is dominated by phonons that, due to electron–phonon coupling, drag electrons in the direction of heat propagation and continue to favor electronic transport. According to Li, et al. [69], the broadening of the G_{inner} sub-band implies a strong electron–phonon coupling; as a consequence of this, as demonstrated in the Raman spectrum of Figure S1 of the Supplementary Materials and in the FWHM variation of Figure 5b, in this study, there was more expressive broadening in the Al@Cu/f-CNT (1) wire than in the Al@Cu/f-CNT (2) wire, which was in line with the higher electrical conductivity presented.

4. Conclusions

The 1350 aluminum alloy conductive wire was successfully coated with Cu/f-CNT via electrophoresis with a current level of 1.2 A, resulting in the creation of the nanostructured Al@Cu/f-CNT (1) wire, whose CNT were surrounded by pyramid structures and clusters of copper and CNT electrodeposited homogeneously on the aluminum substrate, with copper films being cultivated in directions (111) and (220) that favored the formation of thin films with good crystallinity. The addition of iodine in the electrophoretic solution caused a doping effect on the f-CNT surface, as confirmed by Raman spectroscopy, with redshifts in the G_{inner} and G_{outer} sub-bands. At room temperature, this doping effect, together with the contribution of the excellent properties of CNT, resulted in an increase in the electrical conductivity of the nanostructured wire of approximately 18% as compared to the conventional wire, due to the favoring of charge transfer and the formation of new metallic conduction channels. With heating from 25 to 50 °C over 18.5 min, the conductivity of the Al@Cu/f-CNT (1) wire was reduced by around 6.23%, with this being above the value recorded for the AA 1350 wire at 25 °C; this is very important for cable conductors operating in extremely hot climate environments. These results demonstrate that the coating of conductive aluminum wires with the Cu/f-CNT system is promising for applications in power transmission lines, and it could also be adapted for applications in areas such as electrical connections and electronic components.

Supplementary Materials: The following supporting information can be downloaded at: https://www.mdpi.com/article/10.3390/met12050787/s1, FigureS1: Raman Spectrum of (a) f-CNT, (b) Al@Cu/f-CNT (1) and (c) Al@Cu/f-CNT (2) samples; FigureS2: SEM micrographs of (a) Al@Cu/f-CNT (1) and (b) Al@Cu/f-CNT (2) wires, coated by electrophoresis for 8 min with electric currents of 1.2 A and 1.5 A, respectively. Micrographs with 667× magnification obtained via secondary electrons, with a voltage of 20 kV and working distances of (a) 15.34 mm and (b) 15.00 mm; FigureS3: (a) Shifts and (b) FWHM variations of the $2D_{inner}$ and $2D_{outer}$ sub-bands of the samples; FigureS4: Comparison between the electrical resistivities of conventional and nanostructured wires, at room temperature.

Author Contributions: F.R.: Conceptualization, methodology, investigation, interpretation and discussion of results, writing—original draft preparation. P.P.: methodology, interpretation and discussion of results, writing—original draft preparation. R.A.: methodology, investigation, writing—

original draft preparation. S.P.: methodology, investigation, writing—original draft preparation. M.S.: methodology, investigation, interpretation and discussion of results, writing—original draft preparation. M.R.: Conceptualization, methodology, investigation, interpretation and discussion of results, writing—review and editing. All authors have read and agreed to the published version of the manuscript.

Funding: PROPESP/UFPA (PAPQ).

Data Availability Statement: Not applicable.

Acknowledgments: P.P. and M.S. thank CNPq and the Ministry of Regional Development, respectively, for their individual financial support. The authors thank the Laboratory of Characterization of Metallic Materials of FEM/UFPA, the Laboratory of Mineral Characterization in the X-ray sector of the PPGG/UFPA and the Laboratory of Vibrational Spectroscopy and High Pressures of the PPGF/UFPA for their support with SEM, XRD and Raman Spectroscopy characterization, respectively. Soli Deo gloria.

Conflicts of Interest: The authors declare no conflict of interest.

References

1. Chen, S.; Fu, S.; Liang, D.; Chen, X.; Mi, X.; Liu, P.; Zhang, Y.; Hui, D. Preparation and properties of 3D interconnected CNTs/Cu composites. *Nanotechnol. Rev.* **2020**, *9*, 146–154. [CrossRef]
2. Park, M.; Lee, D.-M.; Park, M.; Park, S.; Lee, D.S.; Kim, T.-W.; Lee, S.H.; Lee, S.-K.; Jeong, H.S.; Hong, B.H.; et al. Performance enhancement of graphene assisted CNT/Cu composites for lightweight electrical cables. *Carbon* **2021**, *179*, 53–59. [CrossRef]
3. Bazbouz, M.B.; Aziz, A.; Copic, D.; Volder, M.; Welland, M.E. Fabrication of High Specific Electrical Conductivity and High Ampacity Carbon Nanotube/Copper Composite Wires. *Adv. Electron. Mater.* **2021**, *7*, 2001213. [CrossRef]
4. Milowska, K.Z.; Ghorbani-Asl, M.; Burda, M.; Wolanicka, L.; Ćatić, N.; Bristowe, P.D.; Koziol, K.K.K. Breaking the electrical barrier between copper and carbon nanotubes. *Nanoscale* **2017**, *9*, 8458–8469. [CrossRef] [PubMed]
5. Daneshvar, F.; Tagliferri, S.; Chen, H.; Zhang, T.; Liu, C.; Sue, H.-J. Ultralong electrospun copper-carbon nanotube compositefibers for transparent conductive electrodes with high operational stability. *ACS Appl. Electron. Mater.* **2020**, *2*, 2692–2698. [CrossRef]
6. Zhao, Y.; Wei, J.; Vajtai, R.; Ajayan, P.M.; Barrera, E.V. Iodine doped carbon nanotube cables exceeding specific electrical conductivity of metals. *Sci. Rep.* **2011**, *1*, 83. [CrossRef]
7. Zhang, S.; Nguyen, N.; Leonhardt, B.; Jolowsky, C.; Hao, A.; Park, J.G.; Liang, R. Carbon-Nanotube-Based Electrical Conductors: Fabrication, Optimization, and Applications. *Adv. Electron. Mater.* **2019**, *5*, 1800811. [CrossRef]
8. Loayza, C.R.L.; Borges, D.J.A.; Cardoso, D.C.S.; Assunção, P.D.C.; Ferreira, V.O.; Baia, P.E.C.; Castro, A.A.F.; Reis, M.A.L.; Braga, E.M. A new approach for the reinforcement of SS 304L via arc welding: Using nanostructured flux cored electrode. *Diam. Relat. Mater.* **2019**, *92*, 138–145. [CrossRef]
9. Agarwal, A.; Bakshi, S.R.; Lahiri, D. *Carbon Nanotubes: Reinforced Metal Matrix Composites*, 1st ed.; CRC Press: Boca Raton, FL, USA, 2011; pp. 19–48.
10. Berber, S.; Kwon, Y.-K.; Tománek, D. Unusually high thermal conductivity of carbon nanotubes. *Phys. Rev. Lett.* **2000**, *84*, 4613. [CrossRef]
11. Cao, A.; Qu, J. Size dependent thermal conductivity of single-walled carbon nanotubes. *J. Appl. Phys.* **2012**, *112*, 013503. [CrossRef]
12. Imtani, A.N. Thermal conductivity for single-walled carbon nanotubes from Einstein relation in molecular dynamics. *J. Phys. Chem. Solids* **2013**, *74*, 1599–1603. [CrossRef]
13. Borges, D.J.A.; Cardoso, D.C.S.; Braga, E.M.; Castro, A.A.F.; Reis, M.A.L.; Loayza, C.R.L. Stainless steel weld metal enhanced with carbon nanotubes. *Sci. Rep.* **2020**, *10*, 17977. [CrossRef] [PubMed]
14. Mignani, A.; Ballarin, B.; Boanini, E.; Cassani, M.C. Simple one step electrochemical preparation of copper nanostructures. *Electrochim. Acta* **2014**, *115*, 537–545. [CrossRef]
15. Chang, Y.; Lye, M.L.; Zeng, H.C. Large-scale synthesis of high-quality ultralong copper nanowires. *Langmuir* **2005**, *21*, 3746–3748. [CrossRef] [PubMed]
16. Abdo, H.S.; Seikh, A.H.; Mohammed, J.A.; Soliman, M.S. Alloying Elements Effects on Electrical Conductivity and Mechanical Properties of Newly Fabricated Al Based Alloys Produced by Conventional Casting Process. *Materials* **2021**, *14*, 3971. [CrossRef] [PubMed]
17. Ata, M.S.; Sun, Y.; Li, X.; Zhitomirsky, I. Electrophoretic deposition of graphene, carbon nanotubes and composites using aluminon as charging and film forming agent. Colloids and Surfaces A: Physicochem. *Eng. Asp.* **2012**, *398*, 9–16. [CrossRef]
18. Lepak-Kuc, S.; Boncel, S.; Szybowicz, M.; Nowicka, A.B.; Jozwik, I.; Orlinski, K.; Gizewski, T.; Koziol, K.; Jakubowska, M.; Lekawa-Raus, A. The operational window of carbon nanotube electrical wires treated with strong acids and oxidants. *Sci. Rep.* **2018**, *8*, 14332. [CrossRef]
19. Boccaccini, A.R.; Cho, J.; Subhani, T.; Kaya, C.; Kaya, F. Electrophoretic deposition of carbon nanotube–ceramic nanocomposites. *J. Eur. Ceram. Soc.* **2010**, *30*, 1115–1129. [CrossRef]

20. Chai, G.; Sun, Y.; Sun, J.J.; Chen, Q. Mechanical properties of carbon nanotube copper nanocomposites. *J. Micromech. Microeng.* **2008**, *18*, 035013. [CrossRef]
21. Arai, S.; Saito, T.; Endo, M. Cu–MWCNT Composite Films Fabricated by Electrodeposition. *J. Electrochem. Soc.* **2010**, *157*, D147–D153. [CrossRef]
22. Daoush, W.M.; Lim, B.K.; Mo, C.B.; Nam, D.H.; Hong, S.H. Electrical and mechanical properties of carbon nanotube reinforced copper nanocomposites fabricated by electroless deposition process. *Mater. Sci. Eng. A* **2009**, *513–514*, 247–253. [CrossRef]
23. Uddin, S.M.; Mahmud, T.; Wolf, C.; Glanz, C.; Kolaric, I.; Volkmer, C.; Höller, H.; Wienecke, U.; Roth, S.; Fecht, H.-J. Effect of size and shape of metal particles to improve hardness and electrical properties of carbon nanotube reinforced copper and copper alloy composites. *Compos. Sci. Technol.* **2010**, *70*, 2253–2257. [CrossRef]
24. Rodrigues, F.A.S.; Paraguassu, W.; Simões, S.; Vieira, M.F.G.; Souza, J.A.S.; Braga, E.M.; Reis, M.A.L. Electrical and tensile properties of carbon nanotubes-reinforced aluminum alloy 6101 wire. *J. Nanosci. Nanotechnol.* **2017**, *17*, 4837–4841. [CrossRef]
25. Besra, L.; Liu, M. A review on fundamentals and applications of electrophoretic deposition. *Prog. Mater. Sci.* **2007**, *52*, 1–61. [CrossRef]
26. Feng, L.; Zhang, Z.; Mai, Z.; Ma, Y.; Liu, B.; Jiang, L.; Zhu, D. A Super-Hydrophobic and Super-Oleophilic Coating Mesh Film for the Separation of Oil and Water. *Angew. Chem.* **2004**, *116*, 2046–2048. [CrossRef]
27. Su, Y.; Zhitomirsky, I. Electrophoretic deposition of graphene, carbon nanotubes and composite films using methyl violet dye as a dispersing agent. *Colloids Surf. A Physicochem. Eng. Asp.* **2013**, *436*, 97–103. [CrossRef]
28. Li, Y.; Fahrenthold, E. Ab Initio Study of Iodine-Doped Carbon Nanotube Conductors. *J. Eng. Mater. Technol.* **2018**, *140*, 021008. [CrossRef]
29. Rodríguez-Salinas, J.; Hernández, M.B.; Cruz, L.G.; Martínez-Romero, O.; Ulloa-Castillo, N.A.; Elías-Zúñiga, A. Enhancing Electrical and Thermal Properties of Al6061 Parts by Electrophoresis Deposition of Multi-Walled Carbon Nanotubes. *Coatings* **2020**, *10*, 656. [CrossRef]
30. Wavrik, J.F.A.G.; Lourenço, C.R.S.H.; Sebrão, M.Z.; Lourenço, P.M.; Moreira, P.L.F. Corrosão Interna em Cabos Condutores de Linhas de Transmissão de Energia Elétrica: Caracterização da Atmosfera e Técnica para Identificação de Falhas. In Proceedings of the Anais do V Congresso de Inovação Tecnológica em Energia Elétrica (V CITENEL), Belém, PA, Brazil, 22–24 June 2009.
31. Lienig, J. Electromigration and its impact on physical design in future technologies. In Proceedings of the 2013 ACM International Symposium on Physical Design (ISPD'13), Stateline, NV, USA, 24–27 March 2013; pp. 33–40. [CrossRef]
32. Subramaniam, C.; Yamada, T.; Kobashi, K.; Sekiguchi, A.; Futaba, D.N.; Yumura, M.; Hata, K. One Hundred Fold Increase in Current Carrying Capacity in a Carbon Nanotube-Copper Composite. *Nat. Commun.* **2013**, *4*, 2202. [CrossRef]
33. Queiroz, L.M.O. Estimação e Análise das Perdas Técnicas na Distribuição de Energia Elétrica. Ph.D. Thesis, Faculdade de Engenharia Elétrica e de Computação, Universidade Estadual de Campinas, Campinas, Brazil, 2010.
34. Rodrigues, C.E.M.; Tostes, M.E.L.; Bezerra, U.H.; Soares, T.M.; Matos, E.O.; Soares Filho, L.S.; Silva, E.C.S.; Rendeiro, M.F.; Moura, C.J.S. Technical Loss Calculation in Distribution Grids Using Equivalent Minimum Order Networks and an Iterative Power Factor Correction Procedure. *Energies* **2021**, *14*, 646. [CrossRef]
35. Agência Nacional de Energia Elétrica. *Relatório–Perdas de Energia na Distribuição–1/2021*; Agência Nacional de Energia Elétrica: Brasília, Brazil, 2021. Available online: https://www.aneel.gov.br/documents/654800/18766993/Relat%C3%B3rio+Perdas+de+Energia_+Edi%C3%A7%C3%A3o+1-2021.pdf/143904c4-3e1d-a4d6-c6f0-94af77bac02a (accessed on 10 February 2022).
36. Tehrani, M. Advanced Electrical Conductors: An Overview and Prospects of Metal Nanocomposite and Nanocarbon Based Conductors. *Phys. Status Solidi A* **2021**, *218*, 2000704. [CrossRef]
37. American Society for Testing and Materials. *B3-13: Standard Specification for Soft or Annealed Copper Wire*; American Society for Testing and Materials: West Conshohocken, PA, USA, 2018.
38. American Society for Testing and Materials. *B193−20: Standard Test Method for Resistivity of Electrical Conductor Materials*; American Society for Testing and Materials: West Conshohocken, PA, USA, 2020.
39. Reis, M.A.L.; Sousa, M.E.S.; Ferreira, A.A.; Carneiro, I.S.M.; Melo, C.H.; Silva, M.N., Jr.; Vieira, M.F. Effects of CNTs addition on the microstructure and microhardness of stainless steel alloy/carbon-manganese non-alloyed steel welding. *J. Compos. Mater.* **2021**, *55*, 3061–3069. [CrossRef]
40. Mohamed, A.R.; Bahru, R.; Yeoh, W.-M.; Yaacob, K.A. Dimethyl formamide as Dispersing Agent for Electrophoretically Deposited of Multi-Walled Carbon Nanotubes. *Int. J. Petrochem. Sci. Eng.* **2016**, *1*, 13–16. [CrossRef]
41. Lau, C.H.; Cervini, R.; Clarke, S.R.; Markovic, M.G.; Matisons, J.G.; Hawkins, S.C.; Huynh, C.P.; Simon, G.P. The effect of functionalization on structure and electrical conductivity of multi-walled carbon nanotubes. *J. Nanopart. Res.* **2008**, *10*, 77–88. [CrossRef]
42. Marcelino, J.E.M.; Santiago, E.V.; Téllez, G.L.; López, S.H. Chemical Functionalization of Carbon Nanotubes and its Effects on Electrical Conductivity. *J. Nano Res.* **2014**, *28*, 51–61. [CrossRef]
43. Behabtu, N.; Young, C.C.; Tsentalovich, D.E.; Kleinerman, O.; Wang, X.; Ma, A.W.K.; Bengio, E.A.; Waarbeek, R.F.; Jong, J.J.; Hoogerwerf, R.E.; et al. Strong, Light, Multifunctional Fibers of Carbon Nanotubes with Ultrahigh Conductivity. *Science* **2013**, *339*, 182–186. [CrossRef]
44. Li, Y.; Sun, J.Z.; Bian, C.; Tong, J.H.; Dong, H.P.; Zhang, H.; Xia, S.H. Copper nano-clusters prepared by one-step electrodeposition and its application on nitrate sensing. *AIP Adv.* **2015**, *5*, 041312. [CrossRef]

45. Nikolić, N.D.; Branković, G.; Maksimović, V. Morphology and internal structure of copper deposits electrodeposited by the pulsating current regime in the hydrogen co-deposition range. *J. Solid State Electrochem.* **2012**, *16*, 321–328. [CrossRef]
46. Wei, C.; Wu, G.; Yang, S.; Liu, Q. Electrochemical deposition of layered copper thin films based on the diffusion limited aggregation. *Sci. Rep.* **2016**, *6*, 34779. [CrossRef]
47. He, X.; Xu, X.; Bo, G.; Yan, Y. Studies on the effects of different multiwalled carbon nanotube functionalization techniques on the properties of bio-based hybrid non-isocyanate polyurethane. *RSC Adv.* **2020**, *10*, 2180–2190. [CrossRef]
48. Rashad, M.; Pan, F.; Tang, A.; Asif, M. Effect of Graphene Nanoplatelets addition on mechanical properties of pure aluminum using a semi-powder method. *Prog. Nat. Sci. Mater. Int.* **2014**, *24*, 101–108. [CrossRef]
49. Liu, A.; Shi, Z.; Redd, R.G. Mechanism study of Cu-Zn alloys electrodeposition in deep eutectic solvents. *Ionics* **2020**, *26*, 3161–3172. [CrossRef]
50. Mladenović, I.O.; Lamovec, J.S.; Radović, D.G.; Vasilić, R.; Radojević, V.J.; Nikolić, N.D. Morphology, Structure and Mechanical Properties of Copper Coatings Electrodeposited by Pulsating Current (PC) Regime on Si(111). *Metals* **2020**, *10*, 488. [CrossRef]
51. Yue, S.; Gu, M.; Liu, X.; Zhang, J.; Huang, S.; Liu, B.; Ni, C. Effect of ZnI_2 cosolute on quality and performance of γ-CuI ultrafast scintillation crystal grown via evaporation method in acetonitrile solvent. *Opt. Mater.* **2017**, *66*, 308–313. [CrossRef]
52. Mgheer, T.A.; Abdulrazzak, F.H. Oxidation of multi-walled carbon nanotubes in acidic and basic Piranha mixture. *Front. Nanotechnol.* **2016**, *2*, 155–158. [CrossRef]
53. Song, Y.-J.; Han, S.-B.; Lee, H.-H.; Park, K.-W. Size-Controlled Cu_2O Nanocubes by Pulse Electrodeposition. *J. Korean Electrochem. Soc.* **2010**, *13*, 40–44. [CrossRef]
54. Brito, P.R.O.; Loayza, C.R.L.; Sousa, M.E.S.; Braga, E.M.; Angélica, R.S.; Paz, S.P.A.; Reis, M.A.L. Cast Aluminum Surface Reinforced with Carbon Nanotube via Solubilization Treatment. *Met. Mater. Int.* **2022**, *28*, 802–810. [CrossRef]
55. Reis, M.A.L.; Barbosa Neto, N.M.; Sousa, M.E.S.; Araujo, P.T.; Simões, S.; Vieira, M.F.; Viana, F.; Loayza, C.R.L.; Borges, D.J.A.; Cardoso, D.C.S.; et al. Raman spectroscopy fingerprint of stainless steel-MWCNTs nanocomposite processed by ball-milling. *AIP Adv.* **2018**, *8*, 015323. [CrossRef]
56. Louarn, G.; Trznadel, M.; Buisson, J.P.; Laska, J.; Pron, A.; Lapkowski, M.; Lefrant, S. Raman Spectroscopic Studies of Regioregular Poly(3-alkylthiophenes). *J. Phys. Chem.* **1996**, *100*, 12532–12539. [CrossRef]
57. Araújo, P.T.; Barbosa Neto, N.M.; Sousa, M.E.S.; Angélica, R.S.; Simões, S.; Vieira, M.F.G.; Dresselhaus, M.S.; Reis, M.A.L. Multiwall carbon nanotubes filled with Al_4C_3: Spectroscopic signatures for electron-phonon coupling due to doping process. *Carbon* **2017**, *124*, 348–356. [CrossRef]
58. Pimenta, M.A.; Dresselhaus, G.; Dresselhaus, M.S.; Cançado, L.G.; Jorio, A.; Saito, R. Studying disorder in graphite-based systems by Raman spectroscopy. *Phys. Chem. Chem. Phys.* **2007**, *9*, 1276–1290. [CrossRef] [PubMed]
59. Dresselhaus, M.S.; Dresselhaus, G.; Saito, R.; Jorio, A. Raman spectroscopy of carbon nanotubes. *Phys. Rep.* **2005**, *409*, 47–99. [CrossRef]
60. Jorio, A. Raman Spectroscopy in Graphene-Based Systems: Prototypes for Nanoscience and Nanometrology. *Int. Sch. Res. Notices* **2012**, *2012*, 234216. [CrossRef]
61. Timoshevskii, V.; Ke, Y.; Guo, H.; Gall, D. The influence of surface roughness on electrical conductance of thin Cu films: An ab initio study. *J. Appl. Phys.* **2008**, *103*, 113705. [CrossRef]
62. Eklund, P.C.; Arakawa, E.T.; Zarestky, J.L.; Kamitakahara, W.A.; Mahan, G.D. Charge-transfer-induced changes in the electronic and lattice vibrational properties of acceptor-type GICs. *Synth. Metals* **1985**, *12*, 97–102. [CrossRef]
63. Buonocore, F.; Trani, F.; Ninno, D.; Di Matteo, A.; Cantele, G.; Iadonisi, G. Ab initio calculations of electron affinity and ionization potential of carbon nanotubes. *Nanotechnology* **2008**, *19*, 025711. [CrossRef]
64. ACL Cables PLC. Available online: https://acl.lk/front_img/1502964374ACL_bare_conductor_2015.pdf (accessed on 1 January 2022).
65. Tonkikh, A.A.; Tsebro, V.I.; Obraztsova, E.A.; Suenaga, K.; Kataura, H.; Nasibulin, A.G.; Kauppinen, E.I.; Obraztsova, E.D. Metallization of single-wall carbon nanotube thin films induced by gas phase iodination. *Carbon* **2015**, *94*, 768–774. [CrossRef]
66. Wu, Z.; Han, Y.; Huang, R.; Chen, X.; Guo, Y.; He, Y.; Li, W.; Caia, Y.; Wang, N. Semimetallic-to-metallic transition and mobility enhancement enabled by reversible iodine doping of graphene. *Nanoscale* **2014**, *6*, 13196–13202. [CrossRef]
67. Zubair, A.; Tristant, D.; Nie, C.; Tsentalovich, D.E.; Headrick, R.J.; Pasquali, M.; Kono, J.; Meunier, V.; Flahaut, E.; Monthioux, M.; et al. Charged iodide in chains behind the highly efficient iodine doping in carbon nanotubes. *Phys. Rev. Mat.* **2017**, *1*, 064002. [CrossRef]
68. Qiu, L.; Wang, X.; Tang, D.; Zheng, X.; Norris, P.M.; Wen, D.; Zhao, J.; Zhang, X.; Li, Q. Functionalization and densification of inter-bundle interfaces for improvement in electrical and thermal transport of carbon nanotube fibers. *Carbon* **2016**, *105*, 248–259. [CrossRef]
69. Li, K.; McGuire, M.A.; Lupini, A.R.; Skolrood, L.; List, F.; Ozpineci, B.; Ozcan, S.; Aytug, T. Copper–Carbon Nanotube Composites Enabled by Electrospinning for Advanced Conductors. *ACS Appl. Nano Mater.* **2020**, *3*, 6863–6875. [CrossRef]